Reprinted from ENGINEERING FOR POWER, *Vol. 103, No. 1, January 1981*

Influence of Acceleration on the Critical Speed of a Jeffcott Rotor

H. L. Hassenpflug
Research Associate.

R. D. Flack
Assistant Professor.

E. J. Gunter
Professor.

Department of Mechanical and Aerospace Engineering,
School of Applied Science and Engineering,
University of Virginia,
Charlottesville, VA 22901

The effects of angular acceleration on a Jeffcott rotor have been examined both theoretically and experimentally. The equations of motion were solved via numerical integration. The rotor's response to unbalance was predicted for a number of cases of acceleration and damping. Both amplitude and phase responses were studied. In addition, techniques were developed for identifying system damping from data taken during accelerated runs. The results of the analysis indicate that for high acceleration rates the amplitude response at the critical speed may be reduced by a factor of four or more. The speed at which the peak response occurs can also be shifted by 20 percent or more. Experimentally, a small lightly damped rotor ($\zeta = 0.0088$) was run for several acceleration rates. The peak responses typically agree within 6 percent of theoretical predictions. Also, a beat frequency was observed both theoretically and experimentally after the rotor had passed through the critical speed.

Introduction

The high speed operation of many modern machines necessitates their passing through resonances to attain a specified operating speed. In many cases, to insure that a machine safely traverses a critical speed, the machine is rapidly accelerated. However, the transient nature of the passage through the critical speed generally limits the availability of data concerning the fundamental resonant behavior of the system. A change in operating speed or rate of acceleration can strongly influence the machine's maximum response to unbalance and the speed at which it occurs.

In many cases a rotor is rapidly accelerated from rest to operating speed, thus reducing the destructive effect of the presence of critical speeds. However, the deceleration rates on many machines are not controllable. Since deceleration rates are generally slower than acceleration rates, resonant problems may be encountered on run-down, where they may have been avoided on run-up, causing machine damage.

The phenomenon of acceleration through resonance was investigated analytically via a convolution integral by Lewis [1]. His solution displays the amplitude of vibration as a function of non-dimensionalized operating speed. He employed a forcing function of constant amplitude; i.e., it did not vary with speed as in a real unbalance force. When mass unbalance is considered as a forcing function, the amplitude varies as the square of the operating speed. As a result, his results may lead to significant errors when applied to a rotor system. Furthermore, Lewis deals only with the amplitude of response and does not address the phase relationship between unbalance and rotor response.

Baker [2] studied the acceleration of a rotor using a mechanical analog to solve the model equations. However the range of acceleration rates which he employed was out of range for most machinery. Also, he did not include any predictions for very lightly (but nonzero) damped cases. Unfortunately, these are the machines on which acceleration has the most pronounced effect. Phase relations were also not considered in reference [2].

Meuser and Weibel [3] studied accelerating systems with nonlinear spring rates via a mechanical analog. A constant forcing function was used similar to that in reference [1]. Primarily, this paper deals with the effects of nonlinearities rather than acceleration rates.

Gasch, et al. [4] consider acceleration of a rotor under the assumption of constant torque, allowing the acceleration to vary as torque is absorbed in resonant response. Their work avoids the range of practical application by assuming large unbalance eccentricity and very large acceleration rates. Both of these assumptions fall outside of the realm of most machine applications. Reference [4] also only presents results for the amplitude of the response; phase is not considered, nor is the speed at which maximum response occurs.

In all of the previous works, the thrust of the analysis was on predicting rotor response during acceleration. The objective of this paper is twofold. In addition to looking at rotor response during acceleration, a parameter identification method is developed using data from rotors during acceleration. Particularly, the system damping ratio is determined from the phase angle measurement of an accelerated rotor. It may also be determined by observing the speed shift in maximum response for a known acceleration.

Furthermore, experimental data for a rotor system have not been previously presented (although mechanical analogs were used). Thus, another aim of this paper is to present results from a rotor rig demonstrating the effects of acceleration.

Acceleration rates (and deceleration rates) range from zero to a maximum which has been seen in modern applications. The range of damping covers rotors from the heavily damped ($\zeta = 0.25$) to very lightly damped as might be encountered in a system on ball-bearing supports ($\zeta = 0.01$).

The theoretical solution employs a model based on a speed dependent forcing function as is the case in rotating equipment. Only small values for unbalance eccentricity (and hence constant acceleration rates) have been considered here. This assumption is in general

Contributed by the Gas Turbine Division and presented at the Gas Turbine Conference and Products Show, New Orleans, La., March 10–13, 1980 of THE AMERICAN SOCIETY OF MECHANICAL ENGINEERS. Manuscript received at ASME Headquarters December 14, 1979. Paper No. 80-GT-88.

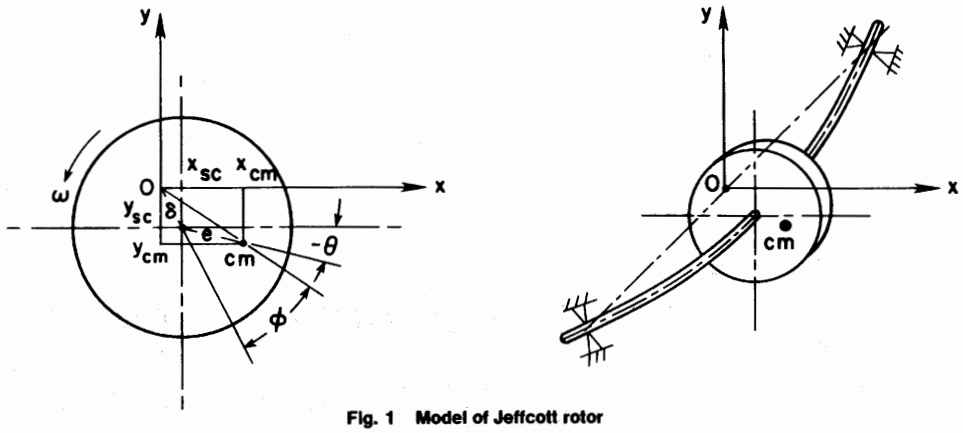

Fig. 1 Model of Jeffcott rotor

quite reasonable. High values of unbalance are quite destructive to machinery and balancing techniques do exist to limit the unbalance in a system to levels where vibration has little effect on acceleration rates. Overall, the aim of this paper is to present results in the range of practicability and applicability to gas turbine rotors and similar systems.

Theoretical Model and Solution

The theoretical model employs a single unbalanced disk, centrally mounted on an elastic shaft which is, in turn, mounted symmetrically on rigid bearings (see Fig. 1). By application of Newton's second law to the system, the following equations of motion are obtained:

$$-KX - CdX/dt = Md^2X_{cm}/dt^2 \tag{1}$$

$$-KY - CdY/dt = Md^2Y_{cm}/dt^2 \tag{2}$$

The coordinates of the disk center of mass, X_{cm} and Y_{cm}, expressed in the fixed coordinates X, Y are

$$X_{cm} = X + e\cos\theta \tag{3}$$

$$Y_{cm} = Y + e\sin\theta \tag{4}$$

Differentiating each of the above equations twice and substituting into equations (1) and (2), the equations of motion are expressed entirely in the fixed coordinate system:

$$\ddot{X} + C\dot{X}/M + KX/M = e(\omega^2\cos\theta + \alpha\sin\theta) \tag{5}$$

$$\ddot{X} + C\dot{Y}/M + KY/M = e(-\omega^2\sin\theta + \alpha\cos\theta) \tag{6}$$

The equations of motion previously derived were simultaneously integrated in time using a standard Euler integration scheme. A similar set of equations was solved by Lewis [1], using a convolution integral. However, the numercial solution has several advantages, one of which is ease of execution. Furthermore, the numerical technique provides versatility in the types of acceleration functions which can be employed (only constant acceleration is presented here). Also, it allows for the solution of phase angle, a formidable analytical problem. The techniques developed here may be applied in more advanced systems with several degrees of freedom for which the convolution integral would be impossible.

The integration procedure used a time step yielding approximately 1/500 revolution per step. Numerical stability was checked by varying step size to as little as 1/25,000 revolution. Results differed by less than one percent.

The results of the integration are expressed in polar coordinates. The instantaneous amplitude of vibration is $\delta = \sqrt{X^2 + Y^2}$. An angle, β, is defined as $\tan^{-1}(Y/X)$. The phase angle, ϕ, is defined as $\phi = \beta - \theta$, which represents the phase difference between the rotor response and unbalance.

The initial conditions for the integration procedure are taken as the unaccelerated or steady-state conditions for a Jeffcott rotor. This technique has the effect of operating for an extended period at some initial speed and then accelerating abruptly.

Unbalance in the system is considered to be small. Non-dimensionally it is represented by e/r_g, where r_g is the disk radius of gyration. For this model, e/r_g was of the order of 10^{-3}. For this range of eccentricity, constant acceleration may be associated with a constant driving torque. Consequently, the energy balance which yields angular acceleration rate as a function of applied torque becomes trivial and is not considered here. Large magnitudes of unbalance ($e/r_g = 0.10$) are examined by Gasch et al. [4], but are in general not representative of unbalances in real machinery. A variety of acceleration rates, both positive and negative, were used here. Also, several cases with different values of system damping were run to demonstrate the effect of damping on the acceleration response.

Theoretical Results

In the previous section, equations were derived for the response of a Jeffcott rotor as it accelerates through the critical speed. In this section, typical results are presented. First, the predicted unbalance response of the rotor is presented for several system parameters cases. Second, it is shown how results from accelerated runs can be used for system parameter identification.

Critical Speed Response. Results of the numerical analysis are presented in several formats. In Figs. 2–5, nondimensionalized amplitude is plotted against the speed ratio, Ω. Each plot has on it several curves, each representing runup at different acceleration rate. The angular acceleration is given nondimensionally by an acceleration ratio, $\gamma = \alpha/\omega_{cr}^2$. Each of the figures covers a different system

Nomenclature

A = amplification factor, δ/e
A_{cr} = critical speed amplification factor at no acceleration, $M\omega_{cr}/C$
A_{max} = maximum amplification factor during acceleration
C = system damping coefficient
e = unbalance eccentricity
K = shaft stiffness
M = mass of the disk
r_g = radius of gyration of the disk
X, Y = shaft displacements
$\dot{X}, \dot{Y}$ = velocities
$\ddot{X}, \ddot{Y}$ = accelerations
α = angular acceleration
γ = acceleration ratio, α/ω_{cr}^2
δ = shaft deflection, $\sqrt{X^2 + Y^2}$
ζ = normalized damping, $1/(2A_{cr})$
θ = angular displacement
ϕ = phase angle
ϕ_{node} = phase angle at "node" (51 or 141 deg)
Ω = speed ratio, ω/ω_{cr}
Ω_{node} = speed ratio at node
ω = angular velocity
ω_{cr} = undamped system critical speed, $\sqrt{K/M}$
ω_{max} = operating speed at A_{max}
ω_{op} = instantaneous operating speed

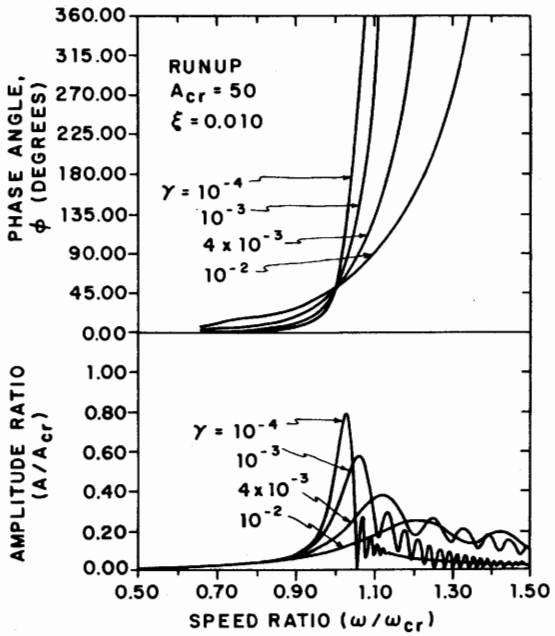

Fig. 2 Critical speed response for runup for $\zeta = 0.010$

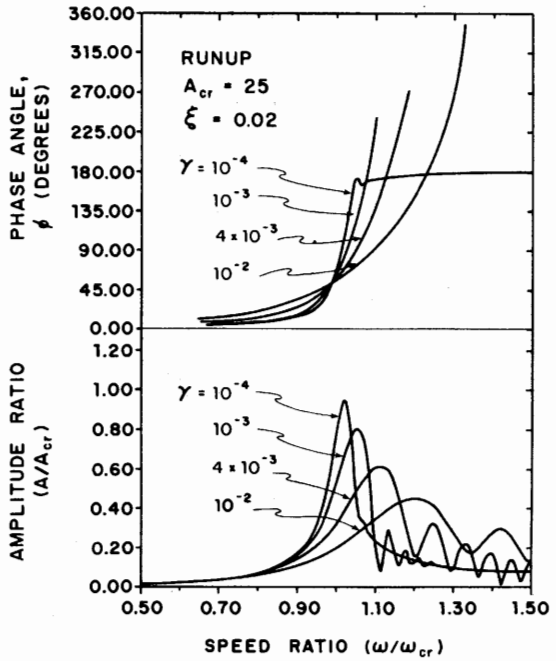

Fig. 3 Critical speed response for runup for $\zeta = 0.02$

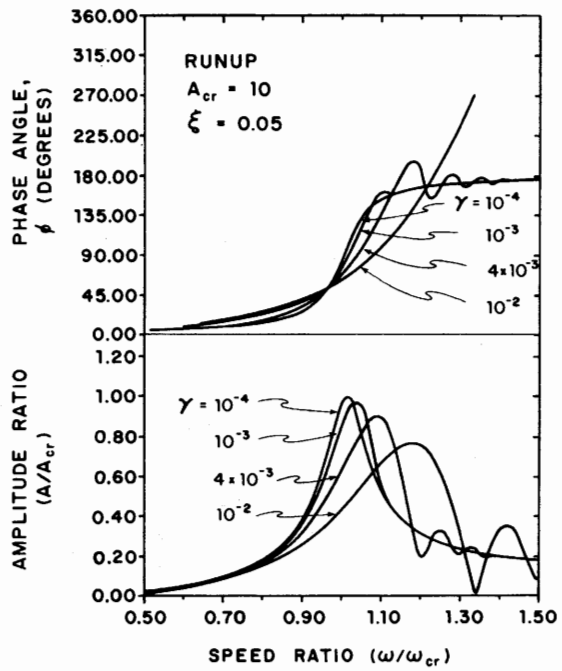

Fig. 4 Critical speed response for runup for $\zeta = 0.05$

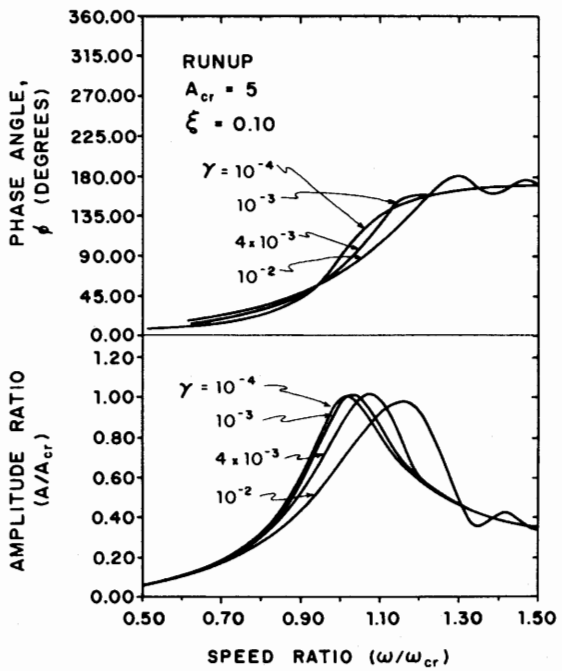

Fig. 5 Critical speed response for runup for $\zeta = 0.10$

damping ratio: $\zeta = 0.10, 0.020, 0.05$, and 0.10. Also in Figs. 2–5, the phase angles are shown, which correspond to the various speeds and acceleration rates. In Fig. 6, several cases of deceleration are considered for a system with a damping ratio, $\zeta = 0.020$. The results are presented in the same manner as in Figs. 2–5.

In each of the amplitude vs speed plots, several phenomena are observed. First, the maximum amplitude of vibration is reduced with the introduction of acceleration or deceleration. Lightly damped systems show the most pronounced reductions in amplitude. Also, the speed at which the maximum amplitude occurs (ω_{max}) is increased with positive acceleration and decreased with deceleration. This effect also is more outstanding in a lightly damped rotor. These phenomena are summarized in Figs. 7 and 8 and are discussed later in this section.

Another peculiarity exhibited by accelerated rotors which is shown by the amplitude plots is a "beating" frequency or harmonic oscillation in the amplitude of vibration, itself. While this behavior has been shown analytically by Lewis [1] and with the aid of a mechanical analog system by Baker [2], neither of their works offers a qualitative explanation of the effect.

This type of rotor behavior is easily explained by the interaction of a free vibration at the system natural frequency, which is excited as the rotor passes through the resonance and a forced vibration at the instantaneous operating speed. Precise measurement of the "beat" frequency shows it to be equal to the difference in operating speed and the critical speed ($\omega_{op} - \omega_{cr}$). The frequency of the "beating" is, therefore, independent of both damping and the acceleration rate. In Figs. 2–6 the beating frequency appears to be dependent on γ. However, one should remember that in these figures, the value of ω_{op} is dependent on both γ and time and thus, the abscissa is not a constant multiple of time for all of the curves.

Only the amplitude of the beat depends on damping. The beating phenomenon is inherently transient as is the free vibration at the critical speed. This is why the beating only occurs in the region of the amplitude plots which follows the critical speed in time, and in heavily damped rotors it is barely noticeable. The accuracy of these results is demonstrated experimentally in the following section.

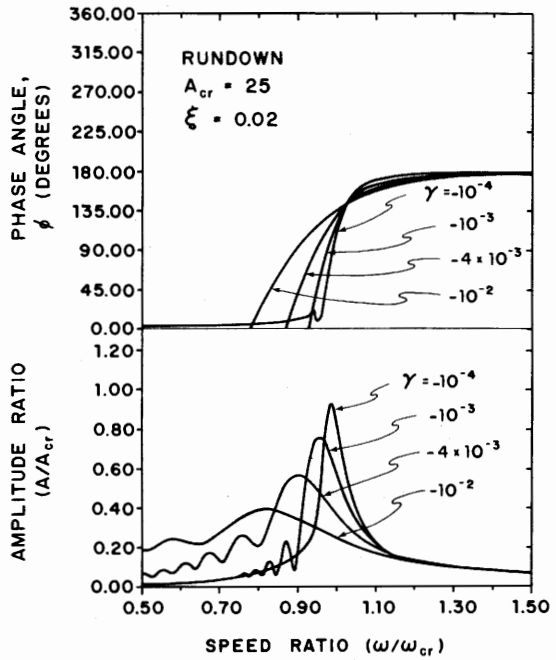

Fig. 6 Critical speed response for rundown for $\zeta = 0.02$

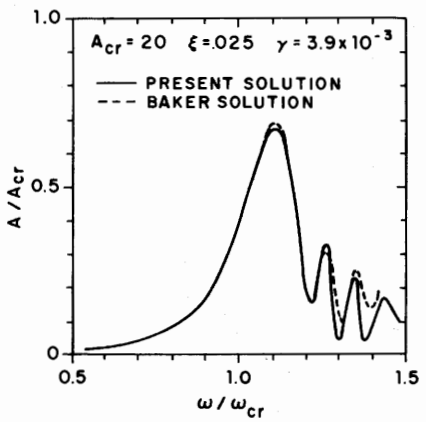

Fig. 7 Comparison of present and Baker [2] critical speed response predictions for runup for $\zeta = 0.025$

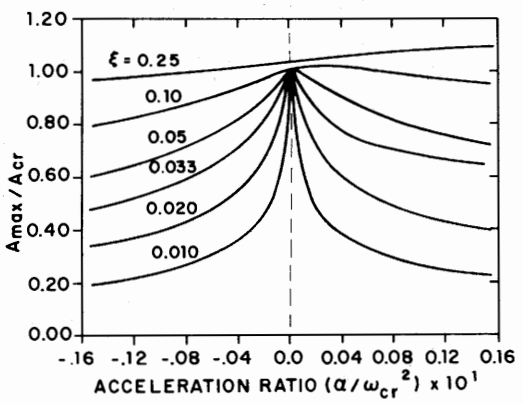

Fig. 8 Summary of maximum amplitude dependence on acceleration rate and damping

The present solution for one case is compared to the analog solution of Baker [2]. Results are shown in Fig. 7 for $\zeta = 0.025$ and $\gamma = 3.9 \times 10^{-3}$. As can be seen, very good agreement is obtained. The difference between the two peak responses is less than 2 percent. The "beating" also occurred at the same frequency.

Looking at the phase relations in Figs. 2–6, several more phenomena can be identified. Unlike the unaccelerated rotor, systems with acceleration do not typically show a 90 deg phase angle at the critical speed. Instead, the phase diagrams show "nodal" points at which the phase is independent of the acceleration rate. One will notice for the case of rundown (Fig. 6) a nodal point occurs above the critical speed, whereas for the cases of runup (Figs. 2–5), the nodal point occurs below the critical speed. In cases of heavy damping both nodal points are seen in both runup and rundown.

Although it has not been proven analytically or numerically, these results strongly suggest that two phase nodal points exist for any system and will be shown unless the phase measurement is obscured by transient vibration as is the case when a rotor undergoes beating. Furthermore, the nodal points are found at $\phi = 51$ deg and $\phi = 141$ deg regardless of damping. The use of these nodal points for system parameter identification will be discussed in the next subsection.

For several of the cases, the phase angle of the total motion is seen to be undefined after the rotor passes through the critical speed. This phenomenon is due to the beating frequency previously described. Two dominant frequencies are present in the system during the beating process. Since the phase angle represents the angle of the synchronous vibration component only, determination of the phase angle of the total motion becomes meaningless; i.e., the predominant frequency of vibration is nonsynchronous.

The results of the rotor response calculations are summarized in Figs. 8 and 9. Figure 8 illustrates the maximum nondimensionalized excursion that a shaft undergoes as a function of acceleration ratio. Several values of system damping are included. Figure 8 represents the vibrational amplitude suppression (or in some cases the magnification) capabilities that accelerating a rotor through a critical speed presents. In Fig. 9, the nondimensionalized speed at which the maximum vibration occurs is presented as a function of α/ω_{cr}^2 for several damping ratios. Figure 9 thus represents the effect rotor acceleration has on the "observed critical speed."

For example, for a rotor with an acceleration ratio of 0.001 and a damping ratio of 0.05, one can expect a maximum response of 78 percent of an unaccelerated case and expect the maximum response at 1.17 times the critical speed. These effects are even more pronounced for lower values of ζ.

Also of interest from Figs. 8 and 9 are the cases with large values of damping. For no acceleration ($\alpha/\omega_{cr}^2 = 0$) and a damping value of $\zeta = 0.25$, the value of A_{max}/A_{cr} is 1.04. The damped critical speed is at 1.07 times the undamped critical speed. As a result of the constant forcing function used by Lewis [1], he found a depressed critical speed. Baker [2] studied only very high acceleration rates ($\gamma \leq 4 \times 10^{-3}$) and, thus, cannot be used for comparison here.

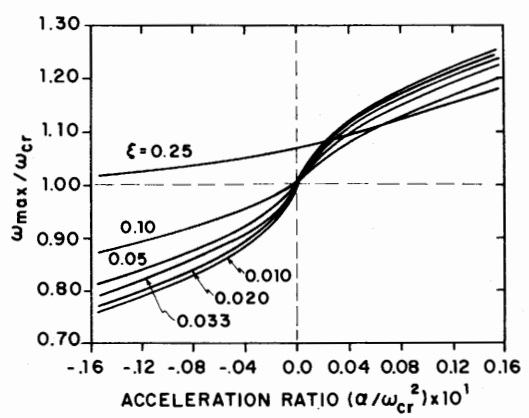

Fig. 9 Critical speed shift as a function of acceleration rate and damping

System Parameter Identification. In the previous subsection the occurrence of "nodal" points on the phase diagrams was determined. These nodes occurred at $\phi = 51$ deg and 141 deg regardless of the value of ζ. In this subsection the use of these conditions to determine the system damping will be discussed.

At the nodal points the relationship for phase is the same as for steady state operation (since all curves for one value of ζ pass through the same point on a ϕ versus ω/ω_{cr} diagram), namely:

$$\tan(\phi_{\text{node}}) = C\,\omega_{\text{node}}/(K - M\omega_{\text{node}}^2) \tag{7}$$

Thus, the damping can be calculated by:

$$\zeta = [(1 - \Omega_{\text{node}}^2)/2\,\Omega_{\text{node}}]\tan(\Omega_{\text{node}}) \tag{8}$$

where $\Omega = \omega/\omega_{cr}$.

To apply the above equations, one must first obtain response plots from a rotor for any acceleration. One next determines the value of the nondimensionalized rotational speed at $\phi = 51$ deg or 141 deg, i.e., Ω_{node}. Once the value of Ω_{node} is determined, ϕ_{node} and Ω_{node} are substituted into equation (8) such that ζ is found.

This method is most easily applied to rotors of significant damping ($\zeta \geq 0.020$). For more lightly damped systems, the nodal points are less than two percent removed from the critical speed and are difficult to accurately distinguish experimentally.

Experimental Results

Critical Speed Response. To demonstrate the accuracy of the results, an experimental analysis was completed. The experimental rig and data analysis system are shown in Fig. 10. The test rotor consisted of a single mass (1.63 kg) centrally located on a 9.53 mm steel shaft. The bearing span was 40.6 cm. The rotational speed was controlled with a 1/6 hp d-c motor. The first critical speed of the rotor was 1730 rpm. On run-up the acceleration rates were constant within 5 percent and on run-down the deceleration rates were constant within 1 percent.

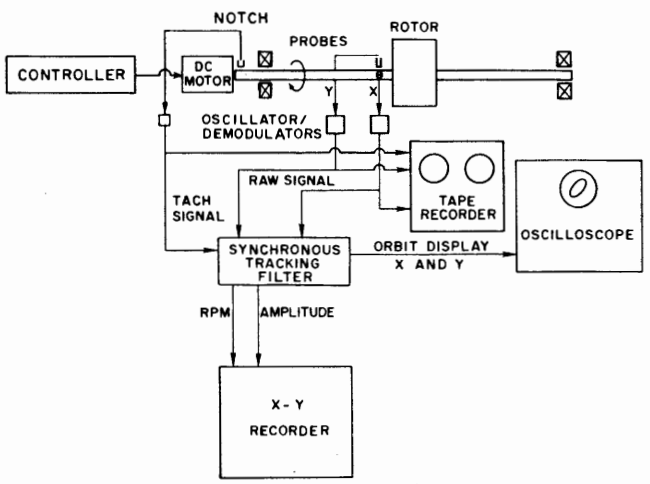

Fig. 10 Test rotor and instrumentation

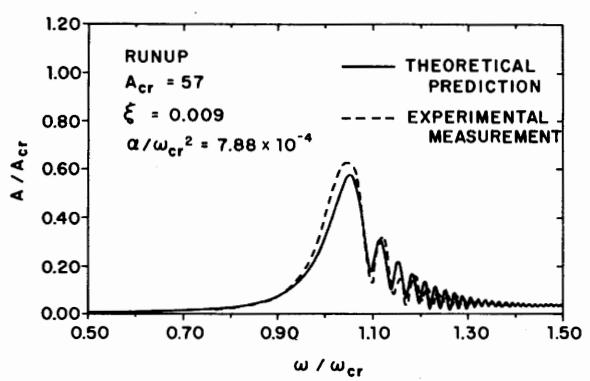

Fig. 11 Typical experimental critical speed response and theoretical predictions

The rig was instrumented with three displacement transducers. Two were located near the mass and the third was placed over a notch on one end of the shaft. The two central probes were calibrated and particular probes were chosen such that the two calibration curves were matched. Thus, direct comparison of the outputs of the X and Y probes was possible.

Data was analyzed using a synchronous tracking filter. The notch on the shaft was used as the trigger for the tracking filter. Outputs from the tracking filter included total or synchronous amplitude and synchronous phase angle (measured with respect to the notch). Reduced data was plotted using an analog plotter. Raw signals from the displacement probes were recorded on an FM tape recorder so that permanent records were obtained.

The rig was first run for no acceleration. A mass unbalance vector of 0.010 mm was used and the bow vector was less than 0.003 mm. From this base run, the system damping was determined. First, the response at the critical speed was divided by the response at four times the first critical speed. The latter corresponds to the mass unbalance vector. This generated a nondimensionalized critical speed response of 59.0, which corresponds to a damping ratio of 0.0085. Secondly, the slope of the phase angle versus speed curve was used to calculate ζ by:

$$\zeta = (d\phi/d\omega)_{cr}^{-1} \times \omega_{cr}^{-1} \tag{9}$$

From equation (9), the value of ζ was found to be 0.0091. Thus, since a difference of less than 7 percent was found, an average of the two methods was used to define the damping: $\zeta = 0.0088$, $A_{cr} = 57$. The bow and unbalance vectors were held constant for the remainder of the tests.

Several tests were performed including acceleration and deceleration runs. One typical run is presented here. For the particular run presented, the value of α/ω_{cr}^2 is 7.88×10^{-4}. The total motion data is presented in Fig. 11. Also presented in Fig. 11 is the theoretical prediction. The damping ratio determined from the baseline case is used in the prediction. As can be seen in Fig. 11, excellent agreement is obtained. First, the theoretical and experimental maximum responses are seen to occur at the same rotational speed ($\omega/\omega_{cr} = 1.050$) and the beating is seen to occur experimentally at the same frequency as predicted. Also, the maximum amplitude (A/A_{cr}) is observed to be 0.62, as compared to the predicted value of 0.58, which results in a difference of 6 percent. Results from other tests were similar and are not presented for brevity.

System Parameter Determination. As a last step, experimental data are presented for a larger rotor mounted in pressure dam journal bearings and the vibration data are used to identify the system damping by three methods. The rotor was a 25.4 mm shaft with single mass of 13.55 kg centrally located. The critical speed of this rotor was 3300 rpm. The motion at the center of the shaft was monitored, and a typical response plot is presented in Fig. 12. The rotor response as well as the test rotor itself is described in reference [5] in detail. In Fig. 12, both the relative phase and magnitude (mm) of the rotor are presented, and this figure is for an acceleration ratio of $\gamma = 1.3 \times 10^{-4}$.

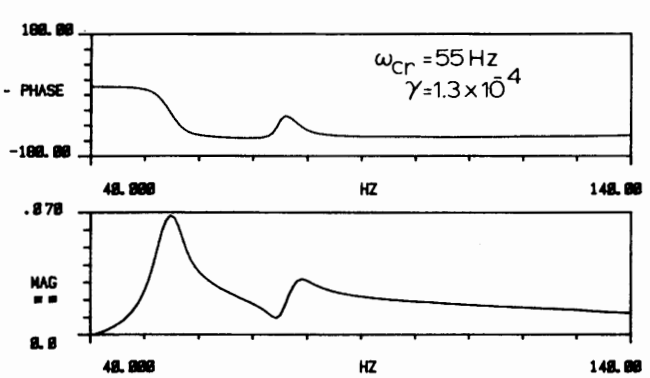

Fig. 12 Data from reference [5] used to demonstrate parameter identifcation

The data for this rotor are analyzed by three methods so that the system damping could be determined. First, the amplification factor was determined at low acceleration rates to be 12.2, by the ratio of the response at the critical speed to the rotor unbalance eccentricity, i.e., $\zeta = 0.041$. Second, the slope of the phase diagram at low acceleration rates yielded a value of ζ from equation (9) to be 0.044. And finally, using the nodal method for $\phi_{node} = 51$ deg (measured with respect to low speeds) yields a ratio of $\Omega_{node} = 0.967$ from Fig. 12. Using these data in equation (8) yields a value of $\zeta = 0.042$. As can be seen, very good agreement is seen with differences less than 5 percent being present between the nodal method and either of the other methods.

Conclusions

Overall, a Jeffcott rotor has been modeled theoretically, and the response (amplitude and phase) of the system as it was accelerated through the critical speed was predicted. A numerical technique was used to solve the equations of motion. If more complex multimass systems are to be examined, such numerical techniques will be necessary as convolution methods will not be practical. Also, experimental data were presented to demonstrate the accuracy of the method. Ranges of system damping, acceleration rates and unbalance eccentricity were studied which are typical in gas turbines and similar machinery. Specific conclusions include:

1 A beating frequency is observed after a rotor passes through the critical speed. The beating represents the difference between the operating and critical speeds.

2 High acceleration rates are seen to affect systems with low damping ratio the most. For systems with $\zeta \gtrsim 0.25$, the maximum response varies by less than 10 percent for practical ranges of acceleration. The speed at which the maximum response is realized is dependent on the acceleration rate, again strongly so for low system damping.

3 A method was developed such that one can use a response phase plot for an accelerated rotor to easily determine the system damping. Such a method was previously not available.

4 Experimental results are presented to demonstrate the accuracy of the predicted responses. Differences between the theoretical and experimental results are less than 6 percent.

5 Experimental results are presented to demonstrate the method of parameter identification for an accelerated rotor. Differences between the presented methods for an accelerated rotor and conventional methods for the same unaccelerated rotor are less than 5 percent.

Acknowledgment

The authors wish to thank Dr. P. E. Allaire for his helpful discussions during this investigation. This research was sponsored by the Department of Energy under contract DE-ACOL-79ET-13151, under the direction of Dr. D. W. Lewis, and the Industrial Supported Program for the Dynamic Analysis of Turbomachinery at the University of Virginia, under the direction of Dr. E. J. Gunter.

References

1 Lewis, F. M., "Vibration During Acceleration Through a Critical Speed," ASME *Journal of Applied Mechanics*, Vol. 54, 1932, pp. 253–257.

2 Baker, J. G., "Mathematical-Machine Determination of the Vibration of an Accelerated Unbalanced Rotor," ASME *Journal of Applied Mechanics*, Vol. 61, 1939, pp. A 145–A 150.

3 Meuser, R. B. and Weibel, E. E., "Vibration of a Non-linear System During Acceleration through Resonance," ASME *Journal of Applied Mechanics*, Vol. 15, 1948, pp. 21-24.

4 Gasch, R., Markert, R., and Pfützner, H., "Acceleration of Unbalanced Flexible Rotors through the Critical Speeds," *Journal of Sound and Vibration*, Vol. 63, No. 3, 1978, pp. 393–409.

5 Flack, R. D., Leader, M. E., and Gunter, E. J., "An Experimental Investigation on the Response of a Flexible Rotor Mounted in Pressure Dam Bearings," accepted for publication in ASME *Journal of Mechanical Design*, 79-JMD-10.